Comparison of molecular dynamics with hybrid continuum–molecular dynamics for a single tethered polymer in a solvent

Sandra Barsky,[a] Rafael Delgado-Buscalioni,[b] and Peter V. Coveney[c]
Centre for Computational Science, Department of Chemistry, University College London, London WC1H 0AJ, United Kingdom

(Received 3 February 2004; accepted 10 May 2004)

We compare a newly developed hybrid simulation method which combines classical molecular dynamics (MD) and computational fluid dynamics (CFD) to a simulation consisting only of molecular dynamics. The hybrid code is composed of three regions: a classical MD region, a continuum domain where the dynamical equations are solved by standard CFD methods, and an overlap domain where transport information from the other two domains is exchanged. The exchange of information in the overlap region ensures that momentum, energy, and mass are conserved. The validity of the hybrid code is demonstrated by studying a single polymer tethered to a hard wall immersed in explicit solvent and undergoing shear flow. In classical molecular dynamics simulation a great deal of computational time is devoted to simulating solvent molecules, although the solvent itself is of no direct interest. By contrast, the hybrid code simulates the polymer and surrounding solvent explicitly, whereas the solvent farther away from the polymer is modeled using a continuum description. In the hybrid simulations the MD domain is an open system whose number of particles is controlled to filter the perturbative density waves produced by the polymer motion. We compare conformational properties of the polymer in both simulations for various shear rates. In all cases polymer properties compare extremely well between the two simulation scenarios, thereby demonstrating that this hybrid method is a useful way to model a system with polymers and under nonzero flow conditions. There is also good agreement between the MD and hybrid schemes and experimental data on tethered DNA in flow. The computational cost of the hybrid protocol can be reduced to less than 6% of the cost of updating the MD forces, confirming the practical value of the method. [DOI: 10.1063/1.1767996]

I. INTRODUCTION

Molecular dynamics (MD) simulations have long been used to model complex fluids both in and out of equilibrium. As computers get more powerful there has been an increasing desire for more chemically accurate models of these fluids. This means that simulations are becoming larger and more accurate, but also that much simulation time is being devoted to model in detail parts of the computational system of little direct scientific interest. One type of hybrid method uses different computational schemes for different types of degrees of freedom within the entire system, e.g., by simulating the polymer with MD and the solvent with lattice Boltzmann,[1] stochastic rotation dynamics,[2] or dissipative particle dynamics.[3] Another family of hybrid methods is based on the spatial decomposition of the system. These schemes combine regions of relatively high degree of chemical accuracy in a specific domain of interest and a more coarse-grained model further away from the specific domain of interest, where the dynamics can be solved in a less computationally intensive way. We focus on this sort of hybrid method and combine Lennard-Jones-type specificity with larger scale continuum methods. Such hybrid methods have been applied in a number of fields, including Lennard-Jones fluids,[4] biophysics,[5] and MD/computational fluid dynamics (CFD) coupling.[6,7] This type of simulation technique is particularly useful in studying interface problems, where the region of interest is a localized part of the entire system.

Typical hybrid methods consist of three regions: a traditional region where dynamics are simulated using well-established techniques such as molecular dynamics,[8] a continuum region where CFD or elasticity differential equations are solved using classical techniques, and an overlap region where the necessary transport information of the MD and continuum regions are exchanged. The primary motivation for using a hybrid scheme is to reduce computer time devoted to simulating bulk regions of little direct interest. As such, a hybrid scheme is ideally suited to studying interfacial systems.

In this paper we apply a hybrid technique to a single polymer tethered to a wall with explicit solvent. The complex dynamics arising from this system have attracted a degree of interest from experimentalists, who used fluorescence microscopy and videomicroscopy to investigate the dynamic properties of individual DNA chains in a shear flow, either tethered to a wall[9] or free.[10] These experiments reveal that the structural quantities, such as the mean elongation of the polymer, are very sensitive to flow environment and that the dynamical properties depend strongly on the initial confor-

[a]Electronic mail: s.barsky@uc1.ac.uk
[b]Electronic mail: uccarde@uc1.ac.uk
[c]Electronic mail: P.V.Coveney@uc1.ac.uk

mation. Moreover, care needs to be taken to control the finite size effects, such as those due to long-ranged hydrodynamic interaction between the polymer and the walls.[10] This large ''sensitivity'' of the tethered polymer dynamics is in fact a valuable test for the hybrid model. First, the hybrid model reduces the size of the MD simulation box while avoiding finite size effects and, second, the coupling has to be able to perfectly reproduce flows at very small shear rates. As shown in a recent work,[11] this second task is nontrivial because the signal-to-noise ratio of the stress that one needs to communicate from the particle to the continuum system is very small.

The problem of tethered polymers under flow has a geometry which is ideal for a hybrid scheme. The scientific interest lies around the polymer although, in a standard MD simulation, the solvent particles within the bulk flow require most of the computational time. Single polymers in a bath of explicit molecular solvent have been the focus of a great deal of attention in the last decade.[1,12–16] Many of these studies are devoted to examining a free chain in solution in order to make comparisons with theoretical predictions, explore the dynamics regime beyond the short-time dynamics, or extract scaling laws as a function of polymer length or shear flow. In these studies, the solvent is explicity simulated. For example, the study by Dünweg and Kremer[12] uses a polymer of length $L=60$ beads in a bath of 7940 Lennard-Jones spheres. Aust, Kröger and Hess[13] simulate polymers of length $L=10-60$ in systems where the total number of particles including solvent ranges from 1000 to 5832. It is clear in these cases that most of the computational effort is devoted to solving the equations of motion of the solvent particles when the real scientific interest lies in the polymer behavior.

The single polymer we study is tethered to a wall, and a variety of shear rates is imposed as a model interfacial problem to compare classical MD techniques to the hybrid simulation. In classical MD, we sandwich the polymer and solution between two explicit walls and impose periodic boundary conditions in the remaining two directions. The polymer is tethered to the bottom wall, and shear is created by moving the top wall at constant velocity in a direction parallel to the wall. In the hybrid case, we model one wall, the polymer, and some of the solvent explicitly using MD, and impose shear by a boundary condition in the CFD regime of the calculation. The shear is translated to the MD regime via energy and momentum flux transfers in the overlap region. We compare various conformational properties of the polymer for the two techniques.

Our paper is organized as follows. In the following section we briefly outline both the classical MD simulation and the hybrid simulation techniques. In Sec. III we compare the conformation of the polymer as calculated by each simulation method. The computational costs and benefits of the hybrid scheme are compared to classical MD. We also compare our results to experimental data of tethered DNA under shear flow. We conclude with a discussion in Sec. IV.

II. METHOD

We describe in this section both the molecular dynamics and hybrid dynamics models used in our simulations. The MD part of the hybrid scheme was the same as the classical MD used in the pure molecular dynamics simulations.

A. Molecular dynamics

The polymer model and simulation techniques are similar to those used in previous work.[17,18] The polymer potential is based on the bead-spring model developed by Kremer and Grest.[19] Linear polymers containing $N=60$ beads each are created by linking nearest neighbors on a chain with the potential

$$U_{nn}(r_{ij})=\begin{cases} -\frac{1}{2}kR_0^2\ln[1-(r_{ij}/R_0)^2], & r_{ij}<R_0, \\ \infty, & r_{ij}\geqslant R_0, \end{cases} \tag{1}$$

where r_{ij} is the distance between beads i and j, $R_0=1.5\sigma$, $k=30\epsilon/\sigma^2$, and σ and ϵ set the length and energy scales, respectively. The monomers in the solvent and in the polymer interact through a truncated Lennard-Jones (LJ) potential

$$U_{LJ}(r_{ij})=\begin{cases} 4\epsilon[(\sigma/r_{ij})^{12}-(\sigma/r_{ij})^6], & r_{ij}<r_c, \\ 0, & r_{ij}\geqslant r_c. \end{cases} \tag{2}$$

The cutoff is set at $r_c=2^{1/6}\sigma$ for all fluid particles to produce a purely repulsive interaction between beads.

The bounds of the simulation cell are periodic in the x and y directions, with periods $L_x\cong 38.5\sigma$ and $L_y\cong 33.4\sigma$, respectively. In the z direction the cell is bounded by top and bottom walls. Each wall contains two layers of 1600 spheres strongly tethered to the sites of a (1,1,1) plane of a fcc lattice by harmonic springs of stiffness $\kappa=1320\epsilon\sigma^{-2}$. The wall atoms do not interact with each other, and the wall-fluid interaction is LJ with an increased cutoff of $r_c=1.25\sigma$ and increased energy scale of $\epsilon_{\mathrm{wf}}=\sqrt{1.7}\epsilon$. The increased cutoff and energy ensure sufficient adhesion of the fluid to the wall so that the slip at the wall is minimized for the shear rates considered here. The polymer is anchored to the wall by enforcing the tethering potential, Eq. (1), between the end of the polymer and one wall atom.

The walls are 48σ apart for the pure MD simulation; in the hybrid simulation the molecular dynamics region persists for 19σ. There are sufficient solvent monomers to yield a mean fluid density of $\approx\rho=0.8\sigma^{-3}$ in the center of the simulation cell, although density oscillations are induced within a few σ of the walls.[20]

The equations of motion are integrated using a velocity Verlet algorithm,[8] with a time step $\delta t=0.0075\tau$, where $\tau=\sigma\sqrt{m/\epsilon}$ is the basic unit of time and m is the mass of a monomer. A constant temperature of $k_BT=1.0\epsilon$ is maintained with a Langevin thermostat.[19] To ensure that this thermostat does not bias the velocity profile along the flow direction, the Gaussian white noise and damping terms are only added to the equations of motion for the velocity components normal to the mean flow, that is, y and z directions.[17]

The shear flow in our pure MD simulation is induced by moving the atomistic top wall at a constant speed v_x in the x direction. In the hybrid simulation, a shear boundary condition is used for the continuum regime, and this resulted in shear in the MD regime by the exchange of momentum in the overlap domain. The starting configuration was that of a

single polymer tethered to the wall in an equilibriated solvent. We repeat the simulation for two different starting configurations, i.e., each configuration has a polymer tethered to a different wall atom, and the initial conformation of the polymer is different. The initial polymer configurations were either taken from previous simulations on melts,[18] or generated from a random walk. Although over long periods of time we expect that different starting configurations will give the same configurational averages, previous work[12] has shown that hundreds of different initial configurations are required to arrive at reasonable ensemble averages. In view of this, we used two initial configurations for the pure MD simulations; although this falls short of the number of initial configurations required to achieve ensemble averages, it does give us a window over which to compare the hybrid simulation.

The local shear rate $\dot{\gamma}$ of the fluid is calculated by computing the local change in the x component of velocity v_x as a function of z, i.e., $\dot{\gamma}=\partial v_x/\partial z$. The upper wall velocity was chosen so that the shear rate $\dot{\gamma}$ assumed the values 0.0, 0.0005, 0.001, 0.002, 0.005, and $0.01\tau^{-1}$. Simulations at higher shear rates were created from lower shear rates by increasing the wall velocity or boundary condition and allowing the system to achieve steady state. The simulations were done for at least one million time steps, and the runs of $\dot{\gamma}=0.001\tau^{-1}$ and $0.005\tau^{-1}$ were simulated for at least ten million time steps, corresponding to a total run time of $75\,000\tau$. In the analysis, in the following section, the first 250 000 time steps of data for each given shear rate were ignored to allow the system to reach steady state; this length of time was determined to be the longest time necessary for the system to reach steady state once a new shear rate was imposed.

B. Hybrid dynamics

Our hybrid dynamics code[21] consists of three domains: the particle domain (P) which was solved by the same molecular dynamics method described above, the continuum domain (C) treated by standard continuum fluid dynamics, and an overlap region where information from the other two domains is exchanged. The hybrid scheme is a protocol to exchange fluxes of conserved quantities, specifically mass, momentum, and energy between both classically treated regimes. To implement the two-way flux exchange, the overlap region consists of two different subdomains: the $P\rightarrow C$ and the $C\rightarrow P$ cells. Within the $C\rightarrow P$ region, the fluxes from the continuum domain are imposed on the particle domain, whereas within the $P\rightarrow C$ cell the microscopic fluxes are coarse grained in time and space[21] to supply boundary conditions for the continuum domain.

The spatial decomposition used for the present setup is shown in Fig. 1. The molecular dynamics domain ranges from the atomistic wall at $z\simeq 0$ and extends to $z=l_{CP}=19\sigma$. The continuum fluid dynamics domain comprises $l_{PC}\leqslant z\leqslant L_z$, where $l_{PC}\simeq 14.5\sigma$ is the z coordinate of the $P\rightarrow C$ interface and $L_z=50\sigma$ is the extent of the whole simulation domain. The center of the $P\rightarrow C$ cell is located at $z=13.4\sigma$; it has a volume $V_{PC}=\Delta z_{PC}A$ where $A=L_x\times L_y$ and $\Delta z_{PC}\simeq 2.2\sigma$ is the extension along the z direction. The

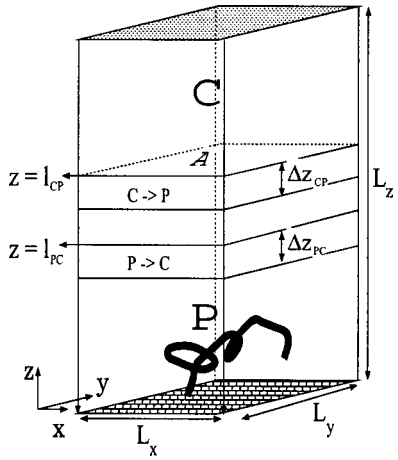

FIG. 1. The domain decomposition of the hybrid scheme. The polymer is embedded within the particle region (P) which is described by molecular dynamics, including the atomistic (lower) wall and the solvent (Lennard-Jones particles). Fluid flow within the continuum region (C) is described by an unsteady Stokes equation and is solved using finite volumes. The handshaking region contains the $C\rightarrow P$ and the $P\rightarrow C$ cell, where the two-way exchange of information is established. The P and C domains overlap within $l_{PC}\leqslant z\leqslant l_{CP}$. The area of the $P\rightarrow C$ and $C\rightarrow P$ cells is the surface of the system in the periodic directions, $A=L_xL_y$. The Couette flow moves along the x direction driven by the velocity imposed by the upper boundary condition, which corresponds to the upper wall velocity in the pure MD simulations, u_{wall}. The magnitudes of each length shown in the figure are given in Sec. II B.

$C\rightarrow P$ cell is placed at a distance 2.2σ from the end of the $P\rightarrow C$ cell and covers a region of $\Delta z_{CP}\simeq 2.2\sigma$ from $z\simeq 16.8\sigma$ to $z=l_{CP}\simeq 19\sigma$.

In what follows we outline the coupling protocol and provide the numerical details used in the present implementation. The $C\rightarrow P$ coupling represents the most complicated part of the hybrid scheme; a more detailed explanation of the method in the frame of the general case of unsteady flows with mass, momentum, and energy exchanges can be found in a previous work.[22] The steady flow considered here only carries momentum along the x direction. Although the mean flux of mass and energy across the C and P interfaces is zero, fluctuations in the particle system produce perturbative mass currents along the z direction which need to be taken into account. This part of the $C\rightarrow P$ scheme is presented in Appendix A.

We now focus on how the momentum flux is exchanged between the C and P domains, starting with a discussion of the $C\rightarrow P$ coupling. For the pure Couette shear flow considered here, the momentum flux due to the C flow across any $z=$ const surface is given by

$$\mathbf{\Pi}=P\mathbf{k}-\eta\dot{\gamma}\mathbf{i}, \tag{3}$$

where $P=P(\rho,T)$ is the hydrostatic pressure, η is the dynamic viscosity, and $\dot{\gamma}\equiv\partial v_x/\partial z$ is the shear rate. The value of the dynamic viscosity was measured in a previous pure MD simulation via the standard nonequilibrium procedure;[13,18,23] for $\rho=0.8$ and $T=1.0$ we obtained $\eta=1.75\pm 0.04$. The stress induced by the C flow in the P domain is given by the local momentum flux at the $C\rightarrow P$ interface, $\mathbf{\Pi}_{CP}$. In order to introduce this stress into the molecular dynamics domain we add an external force $\mathbf{F}_{\text{ext}}=-\mathbf{\Pi}_{CP}A$ to

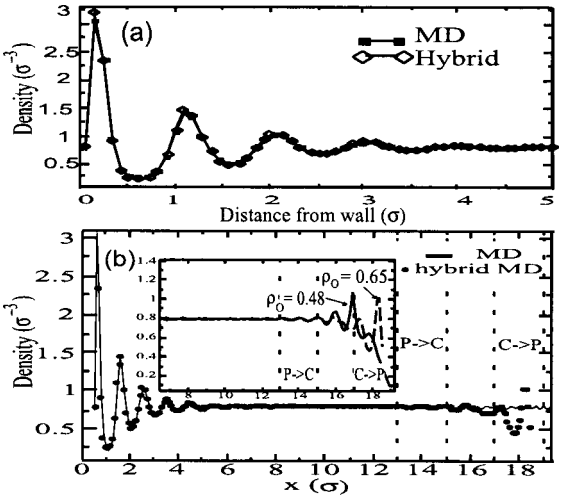

FIG. 2. Monomer and solvent density as a function of distance (z) from the wall for shear rate $\dot{\gamma}=0.005\tau^{-1}$. Part (a) shows the density fluctuations near the lower wall. In (b) dashed lines indicate the locations of the coupling buffers used in the hybrid scheme, $P\rightarrow C$ and $C\rightarrow P$. The inset in (b) compares the density profiles obtained with $\rho_O=0.65$ and $\rho_0=0.48$ in Eq. (A1). In both cases, the bulk density is equal to the desired value, 0.8, and it is unaffected by the hybrid scheme.

those molecules within the $C\rightarrow P$ cell. At any instant of time, t, this force is equally distributed among the $N_{CP}(t)$ particles inside the $C\rightarrow P$ cell; so the external force per particle is $\mathbf{F}_{\text{ext}}/N_{PC}=-\mathbf{\Pi}_{CP}A/N_{CP}$. Note that this external force has a component normal to the $C\rightarrow P$ interface, which provides the hydrostatic pressure, and a tangential component providing the shear stress. The molecules are free to enter or leave the $C\rightarrow P$ region; so the number of molecules within this region, $N_{CP}(t)$, and the value of the overall external force fluctuate in time. The average ''pressure force'' per particle is $P(\rho,T)/(AN_{CP})$, where $N_{CP}\sim 2000$ is the mean number of particles within the $C\rightarrow P$ cell (see Appendix A), $A=L_x\times L_y=1286\sigma^2$, and the pressure $P(\rho,T)$ is given from the equation of state provided by Hess, Kroger, and Voigt:[24] $P(0.8,1)\simeq 6.5\epsilon/\sigma^3$. Such a force prevents the escape of particles and, although it induces some ripples on the density profile over the $C\rightarrow P$ cell, it maintains the correct value of the density along the inner part of the MD domain, as seen in Fig. 2(b) and discussed further in the Appendix A.

The shear force is distributed over the particles in the same way as described above for the pressure force. In this case, the flux of x momentum to be injected in the particle system is $\eta\dot{\gamma}_{CP}$, where $\dot{\gamma}_{CP}$ is the local shear rate of the C flow measured at the $C\rightarrow P$ interface.

We next discuss the $P\rightarrow C$ coupling. The continuum domain is a coarse-grained description of the fluid; therefore any information transferred from the molecular to the continuum system needs to be averaged in space and time. These averages need to be local in the continuum space and time coordinates. To that end, the particle quantities are averaged within the $P\rightarrow C$ cell and over a time interval Δt_{av}. It is important to stress that within the $P\rightarrow C$ cell each particle's dynamics are not directly modified by any external artifact; in other words the motion of each particle is uniquely determined by the usual molecular dynamics scheme. To ensure consistency within the hybrid scheme, Δt_{av} and the volume of the $P\rightarrow C$ cell are restricted.[25] For the steady flow employed in this study, the most compelling condition is to guarantee that the signal-to-noise ratio of the momentum flux is larger than 1 and for that reason Δt_{av} needs to increase as $\dot{\gamma}$ decreases.[11] We used $\Delta t_{av}=100\tau$ for $\dot{\gamma}\leqslant 0.001$ and reduced it gradually to 10τ for the fastest flows considered.

To solve the equations of motion in the continuum domain we used the finite volume formulation[26] because it matches by construction the fluxes across cells. The flow within the continuum region is treated as isothermal, incompressible, and with a uniform pressure; hence the mean x velocity is governed by $\partial v_x/\partial t=\nu\partial^2 v_x/\partial z^2$, where $\nu=\eta/\rho$ is the kinematic viscosity and v_x is the velocity in the x direction. At the top of the simulation cell we impose a smooth wall in the CFD sense. This wall moves at a constant velocity $v_x(L_z,t)=u_{\text{wall}}$ which creates the shear flow in the simulation. For the spatial discretization we used a regular mesh with grid spacing $\Delta z\simeq 1.5\sigma$ and the time step of the continuum solver Δt_C was chosen to guarantee the Courant condition, $\Delta t_C\nu/(\Delta z)^2<1/2$.

The protocol for the $P\rightarrow C$ coupling establishes the boundary condition for the continuum domain at the $P\rightarrow C$ interface, $z=l_{PC}$. The coarse-grained microscopic flux of x momentum across the $P\rightarrow C$ interface, whose expression is given in Ref. 22, is set equal to the corresponding value for the C flow at the $z=l_{PC}$ boundary, $\eta\dot{\gamma}_{PC}$, where $\dot{\gamma}_{PC}\simeq[v_x(l_{PC}+\Delta z)-v_x(l_{PC})]/\Delta z$. This condition gives the desired velocity to be imposed at the boundary $v_x(l_{PC})$. The continuity of velocity is ensured by adding a relaxing term in the flux equation which drives the C velocity at the interface towards the corresponding averaged P velocity (see Refs. 11 and 27 for details). As shown in Ref. 11, the relaxation term does not alter the flux balance and it is particularly useful when dealing with flows having low signal-to-noise ratios (low shear rates) to ensure that fluctuations from P to C do not drive apart the mean particle velocity and the continuum velocity at the overlapping region. As a natural extension, we are planning to extend the present scheme to allow hydrodynamic fluctuations in the continuum region.

III. RESULTS AND DISCUSSION

In this section we compare the conformational behavior of the polymers from the MD and hybrid simulations; we use two independent MD simulations for comparison. We study two MD systems because it is well known[16] that two simulations, or experiments, on a tethered polymer may exhibit considerable variation in conformational behavior, even at rather high shear rates. We conclude this section with a discussion of the computational costs and benefits of the hybrid and classical MD techniques.

In Fig. 3 we show the mean-square end-to-end distance R^2 of the polymer in each of the x, y, and z directions. This is a standard measure of polymer conformation,[28] and its values are related to the values of the radius of gyration. At low shear rates the polymer conformation calculated from the hybrid simulation is well within the measured conformations of the MD simulations. At the highest shear rates, Fig. 3(a) shows the conformation of the hybrid polymer to be

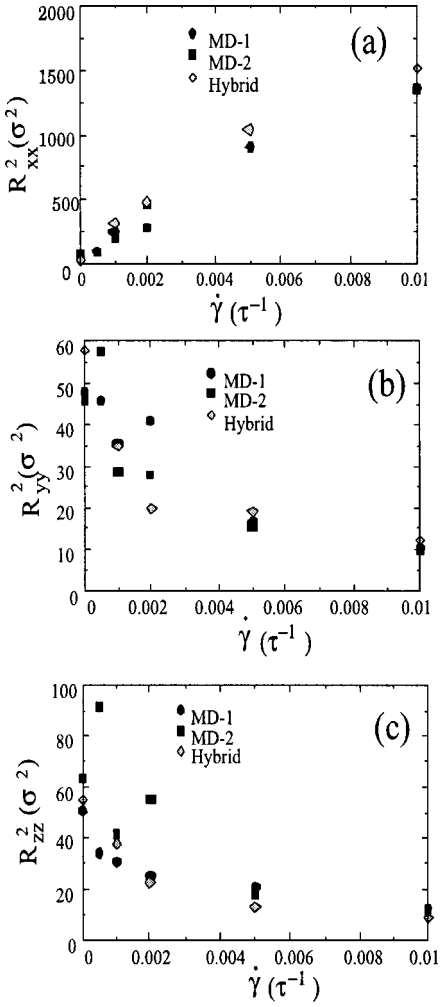

FIG. 3. The x, y, and z components of the mean-square end-to-end vector R^2 are shown as a function of shear rate for two independent MD simulations and one hybrid. Error bars, not shown, are ≈15%. The x component of R^2 increases as the shear rate increases, while the y and z components decrease. At low shear rate the hybrid simulation is well within the variation of the MD simulations. At the highest shear rate the values for R^2_{xx} agree within the measured uncertainty.

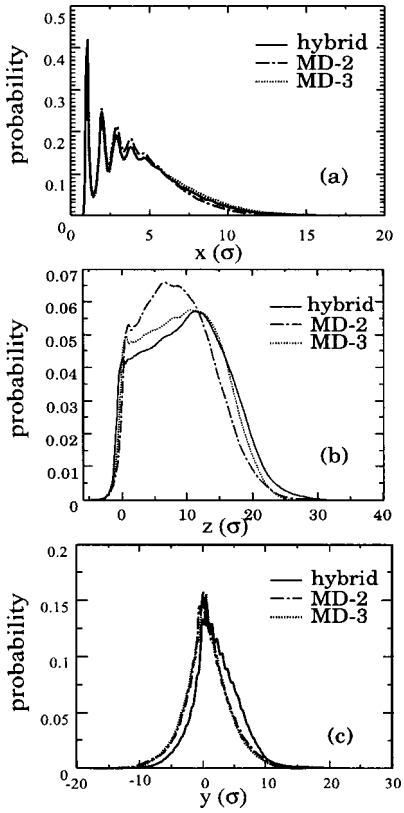

FIG. 4. Probability of finding a monomer in the x (a), y (b), and z (c) coordinates in a flow with shear rate $\dot{\gamma}=0.001\tau^{-1}$. Comparison is made between the result obtained with the hybrid scheme and the outcome of two pure MD simulations with different initial conditions.

about 10% larger than the polymer in the MD simulation; this difference is within the standard deviation of R^2_{xx}, which is about 15%. Figures 3(b) and 3(c) show the y and z components of R^2 as a function of shear rate $\dot{\gamma}$. In both cases the two MD simulations serve as good indicators of the variability of the conformational behavior of a single polymer; the conformation of the polymer in the hybrid simulation is well within the variations found in the two MD simulations at all shear rates.

Figure 4 shows the probability of the maximum extension as a function of distance along x, y, and z directions for a shear rate of $\dot{\gamma}=0.001\tau^{-1}$. It is clear that the variation of the distributions obtained with the hybrid simulation is well within the distribution of the two MD simulations. This indicates that not only is the average conformation comparable between the two simulation techniques but that the probability distributions also compare favorably.

In Fig. 2 we show the density, of both the solution monomers and polymer, $\rho=N/V$ as a function of distance from the wall for both the MD and hybrid simulations. The density is calculated in slices of $\approx 0.01\sigma$ perpendicular to the wall. The regular spacing of the wall monomers, as two monolayers of a (1,1,1) face of a fcc crystal, induces an ordering in the fluid; this ordering is well established[17] and persists for $\approx 5\sigma$. At the wall the monomer density variations are identical for both the MD and hybrid simulations as seen in Fig. 2(a). In Fig. 2(b) we see that the density of both simulations remains the same until the monomers in the hybrid system feel the effects of the constant pressure condition imposed on the overlap region. The constant pressure is implemented as a simple normal force per particle on all monomers in the $C \rightarrow P$ regime, as discussed in the preceding section. As discussed in Appendix A, this force induces a local ordering in the monomers, which in turn creates density fluctuations. It is noteworthy, however, that these density oscillations are much lower than at the atomistic wall, shown for comparison. More recent work on the hybrid scheme has established that we can reduce these density fluctations even further. In the MD simulation, the upper wall is identical to the lower one, and thus the density fluctuations near the former are the same as those at the latter.

Figure 5 shows the probability of finding any polymer bead in a plane, where the plane slices are 0.2σ in thickness. The two-dimensional probabilities were calculated in an analogous way to the one-dimensional probabilities discussed above. The shear rate shown is $\dot{\gamma}=0.001$. Inspection of the two-dimensional bead distributions indicates that be-

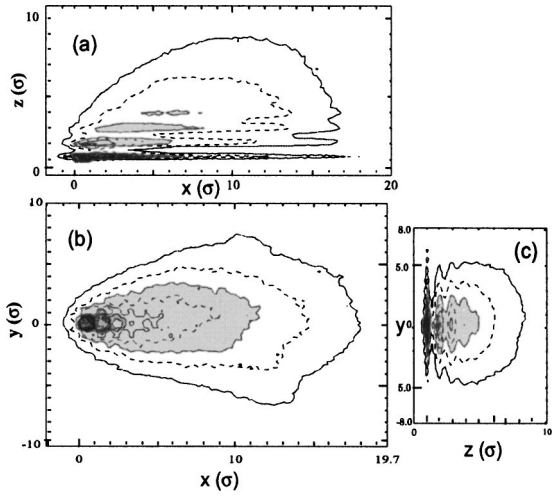

FIG. 5. Probability of finding a monomer in the x-z (a), x-y (b), and y-z (c) planes in a flow with shear rate $\dot{\gamma}=0.001\tau^{-1}$. The maximum of the probability distribution is located near the attachment site. The shaded region corresponds to an isoprobability value of 0.021 and the values of consecutive isoprobability contour lines are separated by 0.01. The histograms were obtained from the calculation of a pure MD simulation with a total simulation time of $78\,750\tau$.

low a distance of $\sim 5\sigma$ to the wall, the beads tend to be ordered in layers parallel to the wall plane. This result is not only a consequence of the polymer-wall interaction but also an effect of the interaction with the solvent. Near the wall the solvent is ordered in layers, as in Fig. 2(a), and the polymer minimizes the monomer-solvent potential energy by adapting its distribution to match the locations of the solvent layers. The order induced by the wall in the polymer structure can be noticed even in the isovalues of the probability distribution along the wall plane x-y, shown in Fig. 5(b), and along the z-y plane in Fig. 5(c). Over a distance of $\sim 6\sigma$ around the attachment position the isovalues of the probability distribution in the x-y plane delineate the minimum energy lines of the wall atoms LJ potential. In this model, the size of the wall atoms was chosen to be the same as those of the monomers and solvent particles 1σ. In view of Fig. 5(b), one might expect that the structure of the polymer is sensitive to modifications in the details of the wall-fluid interaction, owing to either changes in the size of the wall atoms or details of the interaction potential.

In Fig. 6 we present a comparison of the radius of gyration R_g, as calculated from MD simulations in this work and that of Aust, Kröger, and Hess[13] (AKR) who studied a single free polymer in a bath of solvent molecules at a variety of imposed shear rates. The potential used to describe the polymer and solvent is the same in both AKR's work and ours; however AKR used a slightly higher density, $\rho=0.85\sigma^{-3}$, compared to our value of $\rho=0.8\sigma^{-3}$. The simulation of AKR used no walls, so the polymer was free to respond to the imposed shear so as to best lower the free energy of the system. Hence the usefulness of the comparison lies primarily in exploring the effect of the wall on the polymer. We see that at extremely low shear rates the values of the radii of gyration are quite comparable. As the shear rate increases the value of R_g that we calculate becomes much larger than for

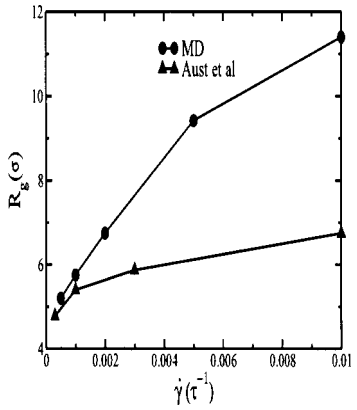

FIG. 6. Comparison of the radius of gyration of the polymer as calculated by MD simulation in this paper, and that of Aust, Kröger, and Hess (Ref. 13) for a free polymer in shear flow.

the equivalent free polymer. This is due to both the grafting of the polymer to the wall and the interaction of the polymer with the wall. We intend to investigate the relative importance of these effects in future work.

Our results are in agreement with the experimental findings of Doyle, Ladoux, and Viovy[9] for individual tethered DNA chains under shear flow. For a quantitative comparison with these experimental data we evaluated the Weissemberg number Wi defined as the product of the shear rate and the longest relaxation time of the polymer, that is, the relaxation time at zero shear rate τ_0. We calculated τ_0 from the autocorrelation of the polymer extension at $\dot{\gamma}=0$ and obtained $\tau_0 \simeq 2000\tau$. Also, the fractional extension was calculated by normalizing the polymer extension with its contour length: $0.965(N-1)$, where $N=60$ is the number of monomers and 0.965σ is the mean separation between two consecutive beads.[29] Using this value of τ_0 we plot in Fig. 7 the mean fractional extension along the flow direction versus the Weissemberg number, along with the experimental results of Doyle *et al.* The results obtained with both the MD and hybrid simulations are in very good agreement with the experimental data for the range of shear rates considered here.

Figure 8 shows the end-to-end volume of the polymer, measured as the product of the three components of the end-to-end vector. This quantity gives an estimate of the space that the polymer explores during its motion. This volume

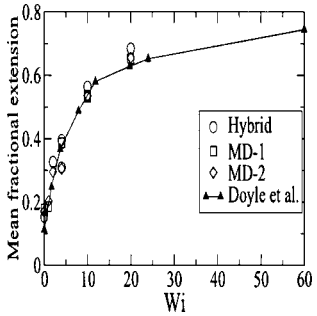

FIG. 7. The fractional elongation along the flow direction vs the Weissemberg number $\mathrm{Wi}=\tau_0\gamma$. The longest decay time at zero shear rate obtained from our data is $\tau_0=2000\tau$. Comparison is made with the experimental results of Doyle, Ladoux, and Viovy (Ref. 9) on tethered polymers.

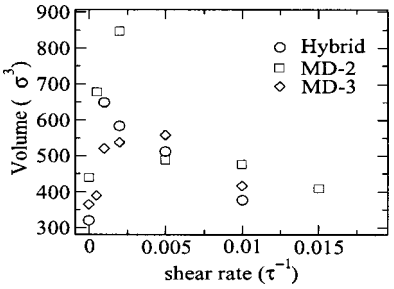

FIG. 8. The end-to-end volume of the polymer as a function of the shear rate. The end-to-end volume is defined by the product of the components of the end-to-end vector, $(R_x^2 \times R_y^2 \times R_z^2)^{1/2}$.

increases for increasing shear rate and reaches a maximum value around $\dot{\gamma} \sim 0.002\tau^{-1}$. As the shear rate is further increased the volume accessible to the polymer decreases monotonically. This behavior of the end-to-end volume is quite similar to the findings of Doyle, Ladoux, and Viovy[9] concerning the amplitude of the fluctuation of the chain extension. As the shear rate was varied, they found that fluctuations reached a maximum size at Wi≃5.1. Using the estimate $\tau_0 \sim 2000\tau$, we find that the maximum end-to-end volume occurs at about Wi∼4. In fact, the size of the fluctuations is determined by the magnitude of the volume made available by the polymer motion; or, in other words, larger fluctuations increase the explored volume. We shall present a more detailed comparison with the results of Doyle, Ladoux, and Viovy[9] in a future work.

There are computational costs to the hybrid method that are not present for classical MD. These include simulating the continuum regime and the calculations arising from the coupling procedure within the overlap region, e.g., particle insertion and deletion and the evaluation of the particle stress tensor. For the flow considered here, the solution of the continuum flow required around 0.01% the time needed for a LJ force calculation. In general, the computational time spent in simulating the continuum region depends on the problem considered, but in any case it will always be much smaller than the MD force evaluation for the solvent. Furthermore, the calculation of the *C* flow occurs once for every ∼20 LJ force calculations, which ensures extra savings in computational time. As shown in Appendix B, the coupling protocol, within the overlap region, is very efficient: only 0.01% of the total computational time was spent in particle insertion and deletion while around 5% in the evaluation of the particle stress tensor. The hybrid code as tested here needs less than half the solvent particles; thus the overall savings in computational time is considerable.

IV. CONCLUSION

In this paper we have compared a newly developed hybrid MD/CFD code to a traditional MD simulation for a single polymer tethered to a wall undergoing shear flow in Couette geometry. We find that the two methods give comparable results for the conformation of the polymer within measured uncertainty.

Our results indicate that the coupling protocol of the hybrid code requires around 5% of the computer time compared to the Lennard-Jones part of the code. Most of the CPU time devoted in the ''coupling'' protocol is spent in the evaluation of the particle momentum flux; while insertion and extraction of particles are rather fast, taking less than 1% of the overall CPU time.

This implies that, compared with a traditional MD simulation, the amount of computational time saved by the hybrid scheme is proportional to the volume of the simulation that is described by the coarse-grained model (CFD). In traditional MD simulations of interfacial phenomena finite size effects significantly alter the local interfacial dynamics, and they can only be reduced by increasing the volume of the simulation box that surrounds the interfacial region of interest. This means that most of the computational cost is likely to be spent in the resolution of the bulk flow. In this paper we have shown that this drawback disappears when using a proper hybrid MD-CFD scheme. To that end, we considered a problem which is very sensitive to small changes in the surrounding fluid environment: the motion of a single tethered polymer under shear flow. The excellent agreement found in the comparisons with the full MD results indicates that the hybrid scheme indeed eliminates finite size effects even in relatively small systems. This means that hybrid simulations can be expected to significantly reduce the computational cost of appropriate interfacial problems.

Apart from the savings in CPU time, the hybrid scheme enables us to gather information from all relevant time and length scales, so it is well suited to treat multiscale problems where bulk fluid flow plays an important role; other examples include crystal growth from fluid phases, wetting phenomena, and membrane dynamics under flow.

We regard the results of the present work as an encouraging sign for future simulations, and we plan to explore various selected interfacial systems in forthcoming research.

ACKNOWLEDGMENTS

We acknowledge fruitful discussions on the hybrid formalism with Eirik Flekkøy. This research was supported by the European Commission through a Marie Curie Fellowship (Grant No. HPMF-CT-2001-01210) and by the EPSRC RealityGrid project, Grant No. GR/R67699. R.D.-B. also acknowledges support from Project No. BFM2001-0290.

APPENDIX A: MASS, LONGITUDINAL MOMENTUM, AND ENERGY FLUCTUATIONS

In this work the mean solvent flow carries no longitudinal momentum along the *z* direction and has a constant mean density. However, we observe that the polymer motion induces density and longitudinal velocity fluctuations within the particle region that induce currents of mass and longitudinal momentum traveling along the simulation box. In order to correctly describe the time-space evolution of these density perturbations one should couple the MD region with the full-blown set of hybrodynamic equations, including fluctuations, i.e., the conservation of mass and energy and the equation for the longitudinal flow.

In this work we have used a simplified approach to control the perturbative currents at the $C \rightarrow P$ interface. The idea

of this approach is to ensure that the mean mass flux across the $z=l_{CP}$ interface vanishes in such a way that pressure waves can leave the simulation box once they reach the $C \rightarrow P$ interface. In flows involving low values of the Mach number (<0.1), the method explained below prevents pressure waves from bouncing back at the $C \rightarrow P$ interface in the MD region.

The average number of particles crossing the $C \rightarrow P$ interface per unit time is given by $\dot{N}_{CP}=A\langle \rho v_z \rangle_{CP}$. The most simple way to ensure zero mass flux is to make this rate equal to the rate of insertion of molecules into the particle system $\dot{N}_{PC}$.[11,21] In the calculations presented here we used another control equation which provides a finer control on the particle density near the $C \rightarrow P$ interface. This approach is based on relaxing the local density at the $C \rightarrow P$ buffer to a prespecified value ρ_O,

$$\dot{N}_{CP}=\frac{V_{CP}}{\tau_m}(\rho_O-\langle \rho \rangle_{CP}), \tag{A1}$$

where V_{CP} is the volume of the $C \rightarrow P$ cell, $\langle \rho \rangle_{CP}$ is the local particle density averaged over Δt_{av}, and τ_m is a relaxation time which controls the rate at which the density fluctuations within $C \rightarrow P$ cell are smoothed out. We set the value of τ_m slightly smaller than the time needed by a sound wave to cross the $C \rightarrow P$ cell [$\sim O(1)\tau$]. In doing so, the fluctuations carrying mass and longitudinal currents through the $C \rightarrow P$ cell are damped and the amplitude of any reflecting wave (which may travel back to the MD domain) is strongly reduced.

According to Eq. (A1), particles are extracted if $\dot{N}_{PC}<0$ and, as explained in previous work,[22] the first particles to be extracted are those closer to the top MD interface at $z=l_{CP}$. If $\dot{N}_{PC}>0$, new particles are inserted with a velocity extracted from a Maxwellian distribution with mean velocity $v_y=v_z=0$ and $v_x=\dot{\gamma}z$ and temperature $T=1.0$. The insertion of particles in liquids is not a trivial task, however, and it is addressed by the USHER algorithm for particle insertion.[21] The value of ρ_O in Eq. (A1) was set to a slightly smaller value, $\rho_O=0.65$, than the mean density 0.8. This choice of ρ_O alleviates some of the computational cost of insertion[30] but, most importantly, it reduces the amplitude and the spatial extent of the density ripples produced near the $C \rightarrow P$ buffer [see Fig. 2(b)]. In fact, if ρ_O is made similar to the bulk density, particles feel the spatial constraint imposed by the top MD interface, thereby inducing larger density fluctuations near $z=l_{CP}=19\sigma$. As shown in Fig. 2(b), using $\rho=0.65$ in Eq. (A1), the density ripples within the $C \rightarrow P$ cell are damped after around 3σ, whereas inside the $P \rightarrow C$ cell the hybrid density profile perfectly matches the density obtained in the pure MD simulation. A perfect match with the bulk density is also obtained when ρ_O is set to a smaller value, as shown in the inset of Fig. 2(b). This means that the condition of constant density at the bulk is guaranteed by the pressure balance between the MD and the continuum domain. Using $\rho_O=0.48$, the end of the $C \rightarrow P$ cell (near $z=l_{CP}\sigma$) becomes rarefied, and density oscillations are larger at the inner $C \rightarrow P$ interface [see Fig. 2(b)]. This indicates that if ρ_O is chosen to be smaller than the bulk density, density oscillations within $C \rightarrow P$ are mainly produced by the external (pressure) force, while the effect of the spatial constraint due to the top MD interface is very small. A more detailed discussion on the end-region density, including some ameliorations of the mass flux boundary condition shall be presented elsewhere.

As long as the fluid is isothermal and there are no mean pressure gradients, the mean energy flux across the $C \rightarrow P$ interface is zero. We therefore only need to guarantee that the specific energy of the newly inserted particles matches that of the ensemble. To ensure the energy balance, new particles are inserted at sites where the interparticle potential energy equals the chemical potential of the system, thereby ensuring the Widom insertion criterion. The kinetic energy is matched by inserting new particles with a Maxwellian distribution, as stated above.

TABLE I. Details of the particle insertion in several hybrid simulations done at shear rate $\dot{\gamma}$. Using ρ_O in Eq. (A1), the average rate of particle insertion was $\dot{N}_{in}$ and the average number of iterations needed by the USHER algorithm to insert a new particle was n_{iter}. E_e is the relative error in the energy upon insertion (the relative difference between the target potential energy and the potential energy at the insertion site). In the last column we show the ratio between the CPU time used by the insertion/extraction subroutines and the CPU time used by the force subroutine plus the Verlet neighbor list.

$\dot{\gamma}(\tau^{-1})$	$\rho_O(\sigma^{-3})$	$\dot{N}_{in}(\tau^{-1})$	n_{iter}	E_e	CPU[insert]/CPU[force]
0.001	0.8	3.68	25.4	0.015	2.7×10^{-4}
0.010	0.8	3.64	25.9	0.015	
0.010	0.65	8.25	14.7	0.006	0.9×10^{-4}
0.005	0.65	4.34	16.3	0.010	

APPENDIX B: COMPUTATIONAL COST OF THE HYBRID METHOD

We compare the computational cost of the coupling subroutines with those pertaining to the MD part of the hybrid scheme. This comparison was made using the GPROF command available in the package of the F77 compiler. One of the parts of the hybrid scheme for which one may expect a certain cost in computational time is particle insertion. Table I presents some results obtained for different shear rates and values of the density ρ_O in Eq. (A1). Typically, Eq. (A1) requires around 5 insertions per time interval τ and around 15 iterations per inserted particle (each interaction involving a single-force evaluation). Therefore, for a time step of $\Delta t_P=0.0075\tau$, the insertion of new particles needs typically about one extra force evaluation per time step. This number is very small when compared with the number of force evaluations needed in the MD system, which is on the order of the number of particles $N_p\sim10^4$. This estimate is consistent with our findings concerning the computational cost. As shown in Table I, in hybrid calculations using $\rho_O=0.65$, the time spent in the insertion/extraction subroutines was about 1.5×10^{-4} times the time spent in the force evaluation and around 0.9×10^{-5} if one includes the Verlet list evaluation. This performance confirms the extremely high efficiency of the USHER algorithm for particle insertion.

As a matter of fact, the dominant cost of the hybrid scheme resides in the evaluation of the particle momentum flux. Its cost in CPU time was about 0.06 times the cost of the force plus Verlet list subroutines. We note that the implementation of this part of our code was not constructed in an efficient way because we evaluated the particle momentum flux at each MD time step. Considering that for the evaluation of $\langle j_p \rangle$ we used measurements of j_p separated by its decorrelation time, about 0.06τ,[11] we could have measured the particle flux roughly every ten time steps and further reduced that ratio by a factor 10. Finally, the time needed to solve the diffusion equation in the continuum domain was very small compared with the MD force subroutine, by a factor of less than 10^{-4}. In general, the computational time required to solve the continuum system will, of course, depend on the specific problem solved.

[1] P. Ahlrichs and B. Dünweg, J. Chem. Phys. **111**, 8225 (1999).
[2] A. Malevantes and J. Yeomans, Europhys. Lett. **52**, 231 (2000).
[3] N. A. Spenley, Europhys. Lett. **49**, 534 (2000).
[4] S. O'Connell and P. Thompson, Phys. Rev. E **52**, R5792 (1995).
[5] G. Ayton, S. Bardenhagen, P. McMurtry, D. Sulsky, and G. A. Voth, IBM J. Res. Dev. **45**, 417 (2001).
[6] J. Li, D. Liao, and S. Yip, Phys. Rev. E **57**, 7259 (1998).
[7] J. Li, D. Liao, and S. Yip, J. Comput.-Aided Mater. Des. **6**, 95 (1999).
[8] M. Allen and D. Tildesley, *Computer Simulations of Liquids* (Oxford University Press, Oxford, 1987).
[9] P. Doyle, B. Ladoux, and J.-L. Viovy, Phys. Rev. Lett. **84**, 4769 (2000).
[10] P. LeDuc, C. Haber, G. Bao, and D. Wirtz, Nature (London) **399**, 564 (1999).
[11] R. Delgado-Buscalioni, P. V. Coveney, and E. Flekkøy (unpublished).
[12] B. Dünweg and K. Kremer, J. Chem. Phys. **99**, 6983 (1993).
[13] C. Aust, M. Kröger, and S. Hess, Macromolecules **32**, 5660 (1999).
[14] C. Pierleoni and J.-P. Ryckaert, Macromolecules **28**, 5097 (1995).
[15] G. G. B. Dünweg and K. Kremer, in *IMA Volumes in Mathematics and Its Applications*, edited by S. Whittington (Springer, New York, 1998), Vol. 102.
[16] R. Jendrejack, J. de Pablo, and M. Graham, J. Chem. Phys. **116**, 7752 (2002).
[17] P. A. Thompson and M. O. Robbins, Phys. Rev. A **41**, 6830 (1990).
[18] S. Barsky and M. O. Robbins, Phys. Rev. E **63**, 021801 (2001).
[19] K. Kremer and G. S. Grest, J. Chem. Phys. **92**, 5057 (1990).
[20] R. Khare, J. J. de Pablo, and A. Yethiraj, Macromolecules **29**, 7910 (1996).
[21] R. Delgado-Buscalioni and P. V. Coveney, J. Chem. Phys. **119**, 978 (2003).
[22] R. Delgado-Buscalioni and P. V. Coveney, Phys. Rev. E **67**, 046704 (2003).
[23] D. J. Evans and G. P. Morris, *Statistical Mechanics of Nonequilibrium Liquids* (Academic, London, 1990).
[24] S. Hess, M. Kroger, and H. Voigt, Physica A **250**, 58 (1998).
[25] As explained in Refs. 22 and 26, these restrictions come from the *C* flow (stability of the scheme and spatiotemporal resolution) and from the *P* system (local thermodynamic equilibrium, signal-to-noise ratio).
[26] S. V. Patankar, *Numerical Heat Transfer and Fluid Flow* (Hemisphere, New York, 1980).
[27] R. Delgado-Buscalioni and P. V. Coveney, Philos. Trans. R. Soc. London (to be published).
[28] M. Doi and S. Edwards, *The Theory of Polymer Dynamics* (Clarendon, Oxford, 1986).
[29] We checked that the monomer separation remains unchanged for the range of $\dot{\gamma}$ considered (it varies in less than 0.005σ).
[30] For a liquid with $\rho \simeq 0.8$ the USHER algorithm needs around 30 iterations to insert a LJ atom at a location where the potential energy equals the mean specific potential energy of the system (Ref. 21). If the density is decreased to 0.65, it only needs about 15 iterations (see Table I).